Lab-on-fiber sensors with Ag/Au nanocap arrays based on the two deposits of Polystyrene nanospheres

Meng Shi *, Shi fang Gao , Liang Shang , Li nan Ma , Wei Wang , Guang qiang Liu , Zong bao Li *

Posted Date: 20 September 2023

doi: 10.20944/preprints202309.1331.v1

Keywords: lab-on-fiber sensor; Ag/Au nanocap arrays; surface-enhanced Raman scattering; polystyrene nanospheres

Article

Lab-on-Fiber Sensors with Ag/Au Nanocap Arrays Based on the Two Deposits of Polystyrene Nanospheres

Meng Shi [1,2,*], Shifang Gao [2], Liang Shang [2], Linan Ma [2], Wei Wang [1], Guangqiang Liu [2] and Zongbao Li [3,4,*]

[1] School of Physical Science and Intelligent Engineering, Jining University, Shandong 273155, China
[2] Shandong Provincial Key Laboratory of Laser Polarization Technology, Qufu Normal University, Qufu 273165 Shandong, China
[3] Ministry of Education Key Laboratory of Textile Fiber Products, School of Materials Science and Engineering, Wuhan Textile University, Wuhan, 430200, China
[4] School of Materials and Chemical Engineering, Tongren University, Guizhou 554300, China
* Correspondence: Authors.E-mail addresses: zongbaoli1982@163.com (Z. Li); philipyes@163.com (M. Shi).

Abstract: Surface-enhanced Raman spectroscopy (SERS) can boost the pristine Raman signal by ~ 10^8 times that could be exploited for producing innovative sensing devices with advanced properties. However, the inherent complexity of SERS systems restricts their further applications in rapid detection, especially in situ detection in narrow aera. Here, we construct an efficient and flexible SERS-based LOP sensor by integrating Ag/Au nanocap arrays obtained by Ag/Au coating polystyrene nanospheres on the optical fiber face. We obtain rich "hotspots" at the nanogaps between neighboring nanocaps and further achieve the excellent SERS performance with the assistance of laser induced thermophoresis on the metal film that can achieve high efficiency aggregation of detected molecules. We achieve a high Raman enhancement with a low detection limitation of 10^{-7} mol/L for the most efficient samples based on the above sensor. This sensor also exhibits good repeatability and stability under multiple detections, revealing the potential application in situ detection based on the reflexivity of optical fiber.

Keywords: lab-on-fiber sensor; Ag/Au nanocap arrays; surface-enhanced Raman scattering, polystyrene nanospheres

1. Introduction

Surface-enhanced Raman spectroscopy (SERS) is considered as one of the most sensitive techniques for non-destructive single-molecular detection with significant advantages of characteristics of fingerprint spectrum and short detection time [1–5]. Despite the mechanism of the chemical and electromagnetic interaction occurring between an analyte and metal nanostructure surface in the SERS detection, the surface area available for analyte detection plays an importance role for SERS that is also one purpose of the conventional SERS substrates constructed with micro/nano-structures [6–8]. Up to data, great efforts have been made to modulate the metal micro/nanostructure on rigid flat-based substrate to achieve high surface area available. However, this kind of SERS sensor lacks integration capabilities limiting its further applications such as in-situ detection in vivo environments.

Lab-on-Fiber (LOF) offers avenues for continued increases in SERS detection based on the advantage of high portable abilities, high biocompatibility and high sensitivity [9,10]. The LOF device can further integrate nanostructure and functional materials on the fiber tip to achieve specific purposes, and are widely used in material analysis [4] biomedical engineering [11], biosensor application [12] and explosive detection [13]. The conventional LOF devices require precise fabrication employing complex nanotechnology, causing high cost of the devices that limited the applications. Developing a low cost but high efficient SERS-based LOF sensors require us to find another way.

 doi:10.20944/preprints202309.1331.v1

Thermophoresis provides an efficient way to achieve collection of molecules or assembly of nanoparticles in solution [14,15]. We can easily achieve the above process only by the incident laser on or off. In our previous works, we successfully obtained the assembly of gold nanoparticles on the LOF platform for SERS detection and developed a photothermal microreactor for copper ion detection using the thermophoresis based on the easy modulated incident power. Coupling SERS hotspots and thermophoresis on a flexible flat-based optical fiber may be the easy way to form low-cost SERS-based LOF sensor.

Ag or Au nanoparticles are widely used to prepare SERS-active substrates and produce rich "hotspot" for SERS enhancement arising from their remarkable surface plasmon properties [16–20]. Meanwhile, the Au or Ag nano-/micro-island will induce thermophoresis in the solution based on the illumination of the launched laser light, benefiting for the analyte transport from other place to the "hotspot" in the solution. Integrated the "hotspot" and the thermophoresis with the optical fiber, we can easily obtain a flexible SERS-based LOF sensor [21,22]. However, the strong oxidizing power of Ag [23] and the weak SERS activity of Au [24] limit the SERS enhancement based on the single noble metal substrate. The Ag/Au bimetallic system integrates the respective advantages and shows both significant Raman signal enhancement and good compatibility, attracting wide attention in the field of SERS [25–28].

Here, we construct a highly efficient and flexible SERS-based LOP sensor by integrating Ag/Au nanocap arrays obtained by Ag/Au coating polystyrene spheres (PS) on the optical fiber facet. The Ag/Au nanocap arrays show obvious hierarchical structure and exhibit strong SERS activity, benefiting for the analyte detection with harmless. We modified the morphologies the Ag/Au nanocap and the thickness of Ag film thickness to optimize the localized surface plasmon resonance (LSPR) effect. The results show that the sensor achieves low detection limits of 10^{-7} mol/L for 4-aminothiophenol (4-ATP) and methylene blue (MB), and 10^{-9} mol/L for Rhodamine 6G (R6G).

2. Experimental

2.1. Materials

The 5 wt% aqueous suspensions of PS spheres with diameter of 120 nm were purchased from Shanghai Hugebio Corporation. R6G, 4-ATP, MB, ethanol are used without further purification.

2.2. Pretreatment of optical fiber

A multimode optical fiber with a core/cladding diameter of 62.5/125 μm is used to prepare fiber-optic SERS sensor. Both ends of the fiber are cleaved using a fiber cutter to obtain flat facets; the fiber is then washed with deionized water and dried in an oven.

2.3. Preparation of Ag/Au nanocap arrays

PS nanospheres with a diameter of 120 nm are arranged on the fiber facet with a perfectly ordered hexagon by employing the gas-liquid interface self-assembly method. Monodisperse polystyrene colloidal particles (5 wt% aqueous suspension) are diluted with ethanol with the ratio of 1:1, then sonicated for 5 min for further use. The colloidal suspension of PS spheres is dropped on one side of the fiber facet, and then the PS colloidal spheres self-assemble into a hexagonal close-packed arrays arising from the attractive capillary force together with the repulsive electrostatic force [29,30]. The monolayer PS sphere film on the glass slide is further formed when deionized water evaporation. An Ag/Au nanofilm is deposited on the top of periodic PS nanospheres by sequence at a rate of 0.02 nm/s by vacuum thermal evaporation technology under a vacuum environment of 5×10^{-4} Pa. Due to the perfectly ordered hexagonal arrangement of PS nanospheres, the Ag/Au film is mainly deposited on the upper half of the PS nanosphere arrays and forms an array of Ag/Au nanogap.

 doi:10.20944/preprints202309.1331.v1

2.4. Characterization

The morphologies of LOF SERS sensor are characterized with a field emission scanning electron microscope (FESEM, Sigma 500). The Raman spectra of the analyte solution are acquired via a portable Raman spectrometer (Ava Spec-ULS-TEC).

2.5. FDTD calculations

The finite-difference time-domain (FDTD) method is used to simulate the electromagnetic field intensity of the LOF SERS sensor. To simplify FDTD stimulation, three adjacent Ag/Au nanocaps are selected as the model.

3. Results and discussion

To achieve the above device for SERE detection, we assembled NPs by using the clean fiber facet and deposit Ag/Au film on the surface to achieve the both photothermal effect and SERS. The details of the preparation process are descripted in the part of the Experimental and schematic presented in Figure 1a. The SEM images in Figure 1b-1d display the perfectly ordered hexagonal arrangement of PS spheres on the fiber facet, producing the possibility of uniform polygonal Ag/Au film on the fiber facet (Figure 1c). In order to obtain the image of nanocap on the PS spheres, we immerse the fiber device in deionized water for ultrasonic cleaning five minutes and obtain the image of an Ag/Au nanocap when nearby nanosphere is removed. As shown in Figure 1d, a bilayer structure of the Ag/Au nanocaps can be clearly recognized from the high magnification SEM images despite the complete overlap of Ag/Au film in polygonal Ag/Au film (Figure 1c) while the Ag/Au bilayer stagger to form nanotriangles' sharp corners which are benefiting for the photothermal effect and SERS [31]. The nanostructure of the bilayer therefore achieves the design goal of the device.

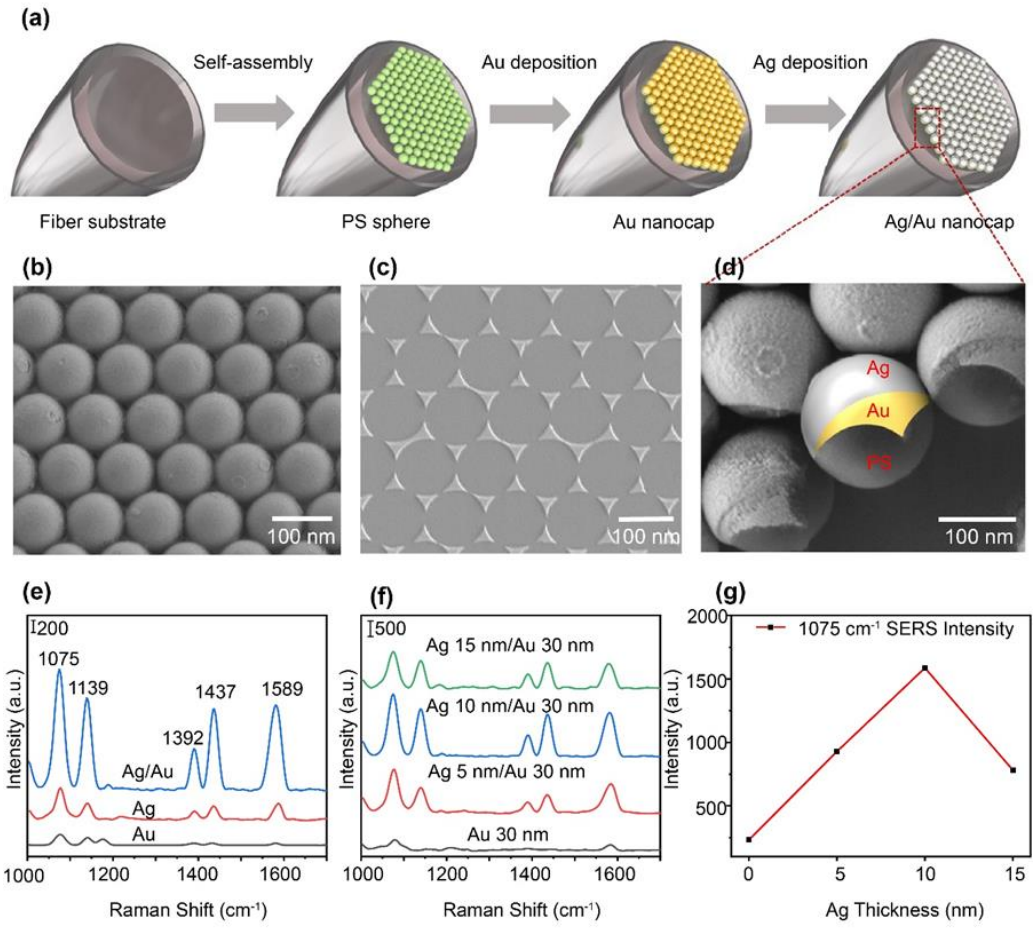

Preprints (www.preprints.org) | NOT PEER-REVIEWED | Posted: 20 September 2023 doi:10.20944/preprints202309.1331.v1

Figure 1. (a) Schematic diagram of the fabrication process of LOF sensor. (b) SEM image of Ag/Au nanocap arrays on the fiber facet. (c) The SEM image of Ag/Au nanotriangles obtained by sonication of Ag/Au-coated nanospheres. (d) The high enlarge SEM image of the Ag/Au nanocap bilayer on the PS sphere surface. (e) 4-ATP (10^{-5} M) Raman spectra obtained from LOF sensor with Ag/Au nanoarrays, Ag nanoarrays and Au nanoarrays. (f) Raman spectra of 4-ATP (10^{-5} M) measured under different conditions of silver film thickness. (g) Corresponding dependence of Raman signal intensity on the thickness of silver.

The composition of the Ag film and Au film is an important factor for Raman signal enhancement. Au monolayer, Ag monolayer and Ag/Au bilayer films are fabricated on the fiber facet by nanosphere lithography. The test system is illustrated in Figure S1. The obtained Raman peaks appear at approximately 1075 cm^{-1}, 1139 cm^{-1}, 1392 cm^{-1}, 1437 cm^{-1} and 1589 cm^{-1} for 4-ATP (10^{-5} M), which are consistent with the previous reports [32,33] and revealing the reliability of the SERS sensor. Compared to both the Ag and Au monolayers, the bilayer film with 30 nm Au and 5 nm Ag exhibit relatively high SERS signal with about 5 times higher than that for Ag monolayer and 10 times than that of the Au monolayer (Figure 1e and S2), revealing the high Raman enhancement of the bilayer film. The significant enhancement property of bilayer film is mainly attributed to the synergic effect of the plasmon from interface of Ag/Au bilayer film.

Furthermore, the thicknesses of the Au and Ag films in the bilayer are the other important factors for SERS enhancement. Employing the 4-ATP (10^{-5} M) as a probe molecule, the enhanced Raman spectra of bilayer films with different Ag thicknesses (0 nm, 5 nm, 10 nm, 15 nm) are presented in Figure 1f. It can be seen that the Raman signal intensity of the 4-ATP changes with the thickness of Ag film. For clarity, the variation of the intensity of the Raman peak at 1074 cm^{-1} 4-ATP solution with a concentration of 10^{-5} M is plotted in Figure 1g. We can see that the SERS peak of the 4-ATP molecule is significantly enhanced when depositing the Ag film on the surface of the Au nanocaps with thickness smaller than 10 nm and then drops with larger thickness of Ag film, revealing the optimum thickness of 10 nm of the Ag film in the bilayer nanocap nanostructure.

The text continues here (Figure 2).

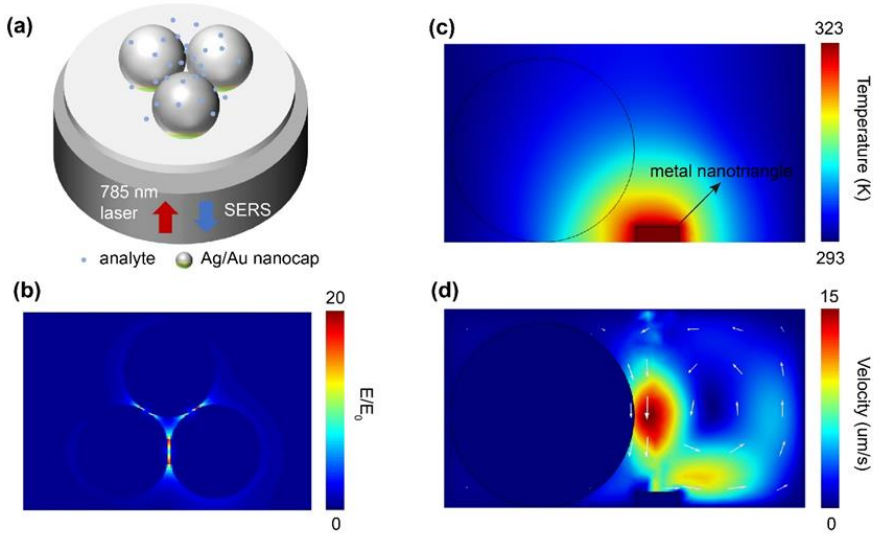

Figure 2. Physical mechanism of SERS-based LOF sensor. (a) Schematic diagram of the LOF sensor based on Ag/Au nanocap on optical fiber facet. (b) Simulated hotspots distributions based on the obtained Ag/Au nanocaps exciting by laser light input from the fiber. Simulation of the thermal field distribution (c) and the liquid velocity field distribution (d) near the metal film on the fiber facet.

Figure 2 schematically presents the physical mechanism of Ag/Au nanogaps on the end face of optical fiber. As shown in Figure 2a, the incident laser light will induce both photothermal appearing at the surface of the Ag/Au film and SERS based on the nanogap between the Ag/Au film. The FDTD

Preprints (www.preprints.org) | NOT PEER-REVIEWED | Posted: 20 September 2023 doi:10.20944/preprints202309.1331.v1

calculations confirm the above assumptions[34]. Under the excitation of 785 nm laser, a rich "hot spot" distribution based on Ag/Au nanocap arrays on the optical fiber facet can be obtained at the nanogaps where the thickness of Ag/Au film is 30 nm/ 5 nm and the diameter of PS microsphere is 120 nm (Figure 2b). The significant field enhancement at the nanogap between adjacent Ag/Au nanocaps is benefit for the SERS. In addition, a 785 nm coupled laser light induces large local heating on both fiber surface and nanocaps where are covered by Ag/Au film. Thanks to the thermophoresis effect, the temperature near the Ag/Au films dissipates gradually from 323 to 293 K (Figure 2c and 2d). The formed local temperature gradient imposes a nonuniform concentrate of the detected molecules that further drive the migration of the molecules in distant solution to the hot region, benefiting for the enhancement of the concentration at the ordered “hot spot” (Figure 2d).

The text continues here (Figure 3).

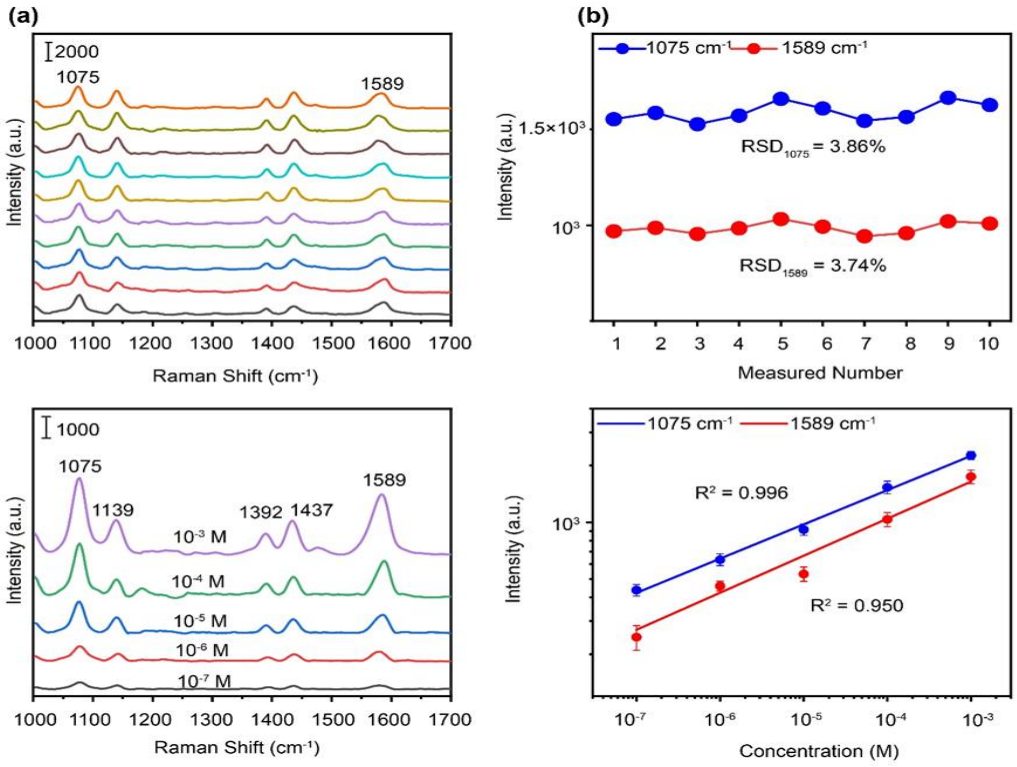

Figure 3. (a) Raman spectra of 4-ATP (10^{-5} M) solution measured by ten LOF sensors. (b) SERS intensities obtained from (a), for peaks at 1075 cm^{-1} and 1589 cm^{-1}. (c) Raman spectra of 4-ATP solutions with concentration of 10^{-3} M to 10^{-7} M, obtained from LOF sensors with Ag/Au nanocap arrays. (d) Log-log plots of SERS intensities versus concentrations at the peak locations of 1075 and 1589 cm^{-1}.

Such an achievement of the nanostructure allows us to characterize the basic SERS properties of this SERS-based LOF sensor. We first select the 4-ATP molecule as the targged molecule to illustrate the LOF sensor performance. Figure 3a displays different SERS spectra based on then sensors using the same 4-ATP solutions with concentration of 10^{-5} M. The SERS intensities of two Raman peaks at 1075 cm^{-1} and 1589 cm^{-1} were plotted in Figure 3b to evaluate the stability of the devices based on the same preparation method. The relative standard deviation values for this two peak intensities are 3.86% and 3.74%, respectively, revealing a high stability and reproducibility.

In order to assess the detection sensitivity of the optimized sensor, the SERS spectra of 4-ATP solutions were recorded at different concentrations from 10^{-3} M to 10^{-7} M in Figure 3c. The results show that a visible SERS peak characteristic of 4-ATP can be observed at concentrations as low as 10^{-7} M, exhibiting an excellent SERS sensitivity. The good linear relationship between the peak intensity (lgI) of 4-ATP’s SERS spectra and the solution concentration (lgC) is presented in Figure 3d with a

Preprints (www.preprints.org) | NOT PEER-REVIEWED | Posted: 20 September 2023 doi:10.20944/preprints202309.1331.v1

coefficient R^2 = 0.996 at 1075 cm^{-1} and R^2 = 0.950 at 1589 cm^{-1}, further confirming the good stability of the sensor. Based on the experimental results, our strategy has been proven to be quantitative in situ detection for low concentration of targeted molecular in a short integration time of 2 s.

For practical applications, it is necessary to study the universality of the SERS sensor on different molecular detections. We thus use this sensor on detection of low-concentration water pollutants, such as the rhodamine 6G (R6G) and methylene blue (MB) as the target molecules. The SERS-based LOF sensor shows sharp and distinct Raman peaks at low concentrations of 10^{-9} M for the R6G solution (Figure 4a, b) and 10^{-7} M for the MB solution (Figure 4c, d), revealing the good Raman enhancement of the sensor for pollutants with low concentrations. The corresponding log-log plots of Raman peaks at 1184 and 1510 cm^{-1} for the R6G solution and at 1398 and 1623 cm^{-1} for the MB solution are further presented in Figure 4b, d, respectively. The good linear relationship between logarithm of intensity and concentration with the R^2 larger than 0.94, confirming the stability of the sensor. Therefore, the SERS-based LOF sensor can be used for quantitative detection of various pollutants with good controllability and high sensitivity.

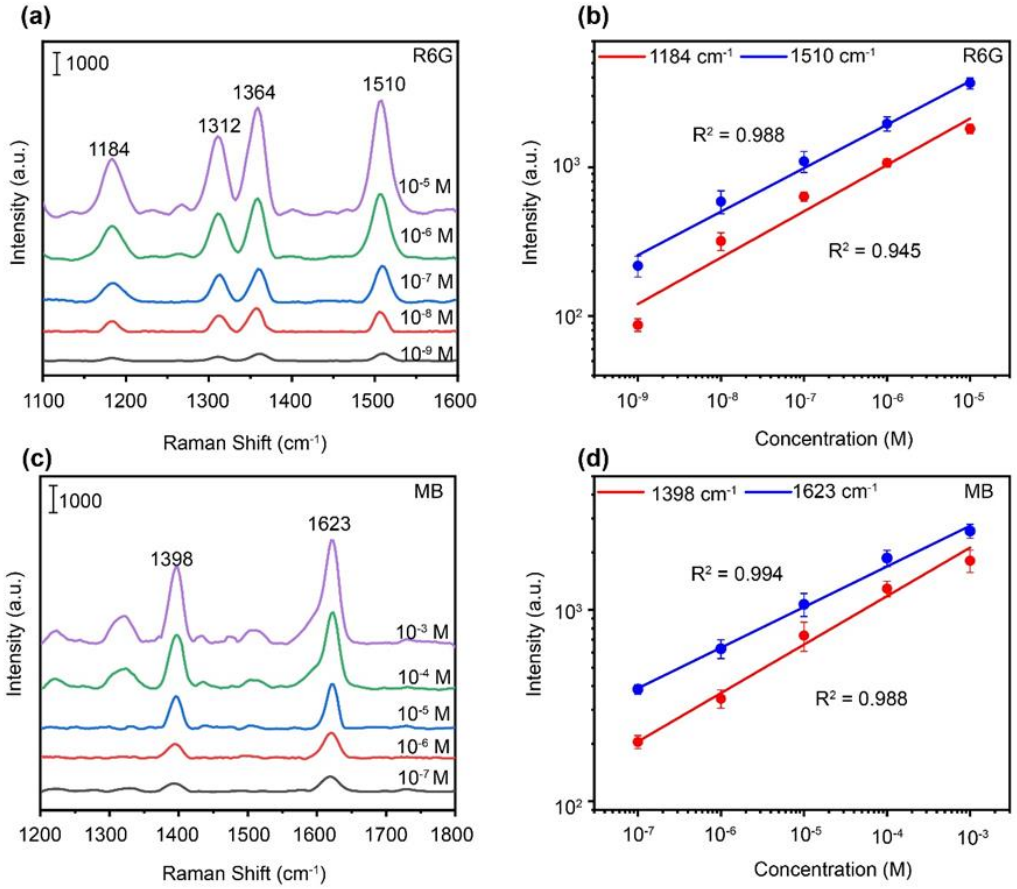

Figure 4. (a) Raman spectra of R6G solution at different concentrations. (b) Log-log plots of SERS intensities versus concentrations at 1184 and 1510 cm^{-1} for the R6G solution. (c) Pamanspectra of R6G solution at different concentrations. (d) Log-log plots of SERS intensities versus concentrations at of 1398 and 1623 cm^{-1} for the MB solution.

The average enhancement factor of the SERS-based LOF sensor can be calculated by the formula $EF = (I_{SERS}/N_{SERS})(I_{RS}/N_{RS})^{-1}$, where I_{SERS} and I_{RS} represent the relative peak intensities of the SERS spectrum from the SERS-based LOF sensor and the Raman spectrum from a naked fiber probe, respectively; N_{SERS} and N_{RS} represent the corresponding numbers of molecules illuminated by the excitation laser in the above two environments [35]. We assume that the volume of analytes near the fiber facet all contributes to the Raman signals. This formula thus can be deviated as $EF = (I_{SERS}/C_{SERS})(I_{RS}/C_{RS})^{-1}$. We noted that, in the measurements, the normal Raman signals of R6G are

difficult to obtain with a bare fiber probe at low concentrations (e.g. 10^{-6} M), so that we applied R6G with a high concentration of 10^{-2} M to obtain the Raman spectrum as shown in Figure S3. The Raman peak intensity at 1510 cm^{-1} is selected to calculate the Raman enhancement factor, and the Raman enhancement factor is calculated to be 2×10^5 for the optimized fiber-optic SERS probes with ordered Ag/Au composite nanostructure, which is about equal to other optical manipulation methods based on Au film deposited glass [36] and plasmonic core-satellite nanostructures [37].

4. Conclusions

In conclusion, we have experimentally and theoretically demonstrated a SERS-based LOF sensor based on the Ag/Au nanogaps on the facet of optical fiber with self-assembly PS spheres. The 10 nm Au film over 35 nm Ag film exhibits the higher Raman enhancement and produce both the photothermal effect. The further experiments confirm the quantitative detection of pollutant solutions, such as 4-ATP, R6G and MB, with the detection limit concentrations of 10^{-7}, 10^{-9} and 10^{-7}, respectively, and reveal the good stability and reliable reproducibility. In the future, we need to combine this microfiber with microfluidic channels to further improve its utility, stability, and recycling efficiency.

CRediT authorship contribution statement: Methodology, Validation, Formal analysis, Investigation, Writing, Visualization, Meng Shi; Methodology, Software, Validation, Formal analysis, Investigation, Writing, Shifang Gao; Investigation. Linan Ma: Investigation, Liang Shang; Methodology, Investigation, Writing, Zongbao Li; Investigation, Wei Wang; Investigation. Xiaobo Xing: Software, Sheng Xue; Resources, Investigation, Guangqiang Liu All authors have read and agreed to the published version of the manuscript.

Declaration of Competing Interest: The authors declare that they have no known competing financial interests or personal relationships that could have appeared to influence the work reported in this paper.

Data Availability: No data was used for the research described in the article.

Acknowledgements: This work was financially supported by the Natural Science Foundation of China (Grant No. 51872161).

References

1. M.E. Farrell, P. Strobbia, P.M. Pellegrino, B. Cullum, Surface regeneration and signal increase in surface-enhanced Raman scattering substrates, Appl. Opt. 56 ,2017; pp. 198–213.
2. H. Huang, J. H. Wang, W. Jin, P. Li, M. Chen, H. H. Xie, X. F. Yu, H. Wang, Z. Dai, X. Xiao, P.K. Chu, Competitive reaction pathway for site-selective sonjugation of Raman dyes to hotspots on gold nanorods for greatly enhanced SERS performance, Small 10 ,2014; pp. 4012-4019.
3. H. Im, K.C. Bantz, S.H. Lee, T.W. Johnson, C.L. Haynes, S. H. Oh, Self-assembled plasmonic nanoring cavity arrays for SERS and LSPR biosensing, Adv. Mater. 25 ,2013; pp. 2678-2685.
4. A. Lucotti, A. Pesapane, G. Zerbi, Use of a geometry optimized fiber-optic surface-enhanced Raman scattering sensor in trace detection, Appl. Spectrosc. 61 ,2007; pp. 260-268.
5. M. Zhang, Y. Lu, L. Zhang, X. Xu, B. Li, X. Zhao, X. Yan, C. Wang, P. Sun, X. Liu, G. Lu, Flexible and wearable glove-based SERS sensor for rapid sampling and sensitive detection of controlled drugs, Sens. Actuators B Chem. 386 ,2023; 133738.
6. S. Fateixa, H.I.S. Nogueira, T. Trindade, Hybrid nanostructures for SERS: materials development and chemical detection, Phys. Chem. Chem. Phys. 17 ,2015; pp. 21046-21071.
7. A. Purwidyantri, I. El-Mekki, C. S. Lai, Tunable plasmonic SERS "hotspots" on Au-film over nanosphere by rapid thermal annealing, IEEE Trans. Nanotechnol. 16 ,2017; pp. 551-559.
8. B.J. Yun, W. G. Koh, Highly-sensitive SERS-based immunoassay platform prepared on silver nanoparticle-decorated electrospun polymeric fibers, J. Ind. Eng. Chem. 82 ,2020; pp. 341-348.
9. A. Lucotti, G. Zerbi, Fiber-optic SERS sensor with optimized geometry, Sens. Actuators B Chem. 121 ,2007; pp. 356-364.
10. Z. Xie, J. Tao, Y. Lu, K. Lin, J. Yan, P. Wang, H. Ming, Polymer optical fiber SERS sensor with gold nanorods, Opt. Commun. 282 ,2009; pp. 439-442.

11. H. Yuan, W. Ji, S. Chu, Q. Liu, S. Qian, J. Guang, J. Wang, X. Han, J.F. Masson, W. Peng, Mercaptopyridine-functionalized gold nanoparticles for fiber-optic surface plasmon resonance Hg(2+) sensing, ACS Sens. 4 ,2019; pp. 704-710.
12. Y. Liu, J. Guang, C. Liu, S. Bi, Q. Liu, P. Li, N. Zhang, S. Chen, H. Yuan, D. Zhou, W. Peng, Simple and low-cost plasmonic fiber-optic probe as SERS and biosensing platform, Adv. Opt. Mater. 7 ,2019; 1900337.
13. R. Bharadwaj, S. Mukherji, Gold nanoparticle coated U-bend fiber optic probe for localized surface plasmon resonance based detection of explosive vapours, Sens. Actuators B Chem. 192 ,2014; pp. 804-811.
14. Z. Zheng, M. Shi, Y. Xu, S. Liu, H. Zhong, Q. Shou, J. Huang, T. Luan, Z. Li, X. Xing, Light-induced dynamic assembly of gold nanoparticles in a lab-on-fiber platform for surface-enhanced Raman scattering detection, ACS Appl. Nano Mater. 5 ,2022; pp. 8005-8011.
15. S. Liu, H. Zhong, Z. Li, Y. Xu, X. Hu, Z. Zheng, L. Liu, P. Chen, X. Cai, X. Jiang, A. Luo, J. Huang, X. Xing, Photothermal microfluidic-assisted self-cleaning effect for a highly reusable SERS sensor, Opt. Lett. 46 ,2021; pp. 4714-4717.
16. G. Liu, W. Cai, L. Kong, G. Duan, Y. Li, J. Wang, Z. Cheng, Trace detection of cyanide based on SERS effect of Ag nanoplate-built hollow microsphere arrays, J. Hazard. Mater. 248 ,2013; pp. 435-441.
17. G. Liu, X. Li, W. Wang, F. Zhou, G. Duan, Y. Li, Z. Xu, W. Cai, Gold binary-structured arrays based on monolayer colloidal crystals and their optical properties, Small 10 ,2014; pp. 2374-2381.
18. S. Yang, X. Dai, B.B. Stogin, T. S. Wong, Ultrasensitive surface-enhanced Raman scattering detection in common fluids, Proc. Natl. Acad. Sci. U. S. A. 113 ,2016; pp. 268-273.
19. G. Liu, Y. Li, G. Duan, J. Wang, C. Liang, W. Cai, Tunable surface plasmon resonance and strong SERS performances of Au opening-nanoshell ordered arrays, ACS Appl. Mater. Interfaces 4 ,2012; pp. 1-5.
20. Y. Zhu, R.A. Dluhy, Y. Zhao, Development of silver nanorod array based fiber optic probes for SERS detection, Sens. Actuators B Chem. 157 ,2011; pp. 42-50.
21. D. Gao, X. Yang, P. Teng, D. Kong, Z. Liu, J. Yang, M. Luo, Z. Li, X. Wen, L. Yuan, K. Li, M. Bowkett, N. Copner, X. Wang, On-line SERS detection of adenine in DNA based on the optofluidic in-fiber integrated GO/PDDA/Ag NPs, Sens. Actuators B Chem. 332 ,2021; 129517.
22. R. Huang, S. Lian, J. Li, Y. Feng, S. Bai, T. Wu, M. Ruan, P. Wu, X. Li, S. Cai, P. Jiang, High-sensitivity and throughput optical fiber SERS probes based on laser-induced fractional reaction method, Results Phys. 48 ,2023.
23. H.W. Yoo, J.M. Jung, S.K. Lee, H.T. Jung, The fabrication of highly ordered silver nanodot patterns by platinum assisted nanoimprint lithography, Nanotechnology 22 ,2011; 095304.
24. Y. Wang, X. Zhao, W. Gao, L. Chen, S. Chen, M. Wei, M. Gao, C. Wang, Y. Zhang, J. Yang, Au/Ag bimetal nanogap arrays with tunable morphologies for surface-enhanced Raman scattering,RSC Adv. 5 ,2015; pp. 7454-7460.
25. T. Zhang, Y. Sun, L. Hang, H. Li, G. Liu, X. Zhang, X. Lyu, W. Cai, Y. Li, Periodic porous alloyed Au-Ag nanosphere arrays and their highly sensitive SERS performance with good reproducibility and high density of hotspots, ACS Appl. Mater. Interfaces 10 ,2018; pp. 9792-9801.
26. T. Liu, X. Xiao, P. Wang, L. Ji, C. Yang, Fiber surface enhanced Raman scattering sensor based on patterned biphasic gold-silver nanoalloys, Chem. Phys. Lett. 553 ,2012; pp. 51-54.
27. Q. Han, C. Zhang, W. Gao, Z. Han, T. Liu, C. Li, Z. Wang, E. He, H. Zheng, Ag-Au alloy nanoparticles: Synthesis and in situ monitoring SERS of plasmonic catalysis, Sens. Actuators B Chem. 231 ,2016; pp. 609-614.
28. Y. Ran, P. Strobbia, V. Cupil-Garcia, T. Vo-Dinh, Fiber-optrode SERS probes using plasmonic silver-coated gold nanostars, Sens. Actuators B Chem. 287 ,2019; pp. 95-101.
29. M. Retsch, Z. Zhou, S. Rivera, M. Kappl, X.S. Zhao, U. Jonas, Q. Li, Fabrication of Large-Area, Transferable colloidal monolayers utilizing self-assembly at the air/water interface, Macromol. Chem. Phys. 210 ,2009; pp. 230-241.
30. J. Yu, Q. Yan, D. Shen, Co-self-assembly of binary colloidal crystals at the air−water interface, ACS Appl. Mater. Interfaces 2 ,2010; pp. 1922-1926.
31. G. Quero, G. Zito, S. Manago, F. Galeotti, M. Pisco, A.C. De Luca, A. Cusano, Nanosphere lithography on fiber: Towards engineered lab-on-fiber SERS optrodes, sensors 18 ,2018; pp. 680.
32. J. Chen, S. Pang, L. He, S.R. Nugen, Highly sensitive and selective detection of nitrite ions using Fe3O4@SiO2/Au magnetic nanoparticles by surface-enhanced Raman spectroscopy, Biosens. Bioelectron. 85 ,2016; pp. 726-733.

33. L. Xing, Y. Xiahou, X. Zhang, W. Du, P. Zhang, H. Xia, Large-area monolayer films of hexagonal close-packed Au@Ag nanoparticles as substrates for SERS-based quantitative determination,ACS Appl. Mater. Interfaces 14 ,2022; pp. 13480-13489.
34. C. Yang, P. Liang, L. Tang, Y. Zhou, Y. Cao, Y. Wu, D. Zhang, Q. Dong, J. Huang, P. He, Synergistic effects of semiconductor substrate and noble metal nano-particles on SERS effect both theoretical and experimental aspects, Appl. Surf. Sci. 436 ,2018; pp. 367-372.
35. E.C. Le Ru, E. Blackie, M. Meyer, P.G. Etchegoin, Surface enhanced Raman scattering enhancement factors: a comprehensive study, J. Phys. Chem. C 111 ,2007; pp. 13794-13803.
36. L. Lin, X. Peng, M. Wang, L. Scarabelli, Z. Mao, L.M. Liz-Marzán, M.F. Becker, Y. Zheng, Light-directed reversible assembly of plasmonic nanoparticles using plasmon-enhanced thermophoresis, ACS Nano 10 ,2016; pp. 9659-9668.
37. C. Y. Kang, J. J. Li, L. A. Wu, C. C. Wu, Y. F. Chen, Dynamic and reversible accumulation of plasmonic core-satellite nanostructures in a light-induced temperature gradient for in situ SERS detection, Part. Part. Syst. Charact. 35 ,2018.